

DOI: 10.24425/118974

M. AKBARZADEH*, M. ZANDRAHIMI*#, E. MORADPOUR**

SYNTHESIS AND CHARACTERIZATION OF MOLYBDENUM DISULFIDE COMPOSITE COATING ON STEEL USING CHEMICAL VAPOR DEPOSITION

Molybdenum disulfide (MoS_2) is one of the most widely used solid lubricants applied in different ways on the surfaces under friction. In this work, AISI 316 austenitic stainless steel was coated with MoS_2 , using chemical vapor deposition (CVD) at four different temperatures (400, 500, 600 and 700°C). Coatings properties were investigated using SEM, EDX, XRD and FTIR, Hardness Tester and Roughness tester. The results showed that with simultaneous evaporation of sulfur and molybdenum trioxide (MoO_3) in the CVD chamber, a uniform coating layer containing MoS_2 and MoO_2 phases was formed. Increase in the substrate temperature resulted in the rise in the amount of MoS_2 to MoO_2 phases. The thickness, grain size and the hardness of the coating were 17-29 μm , 50-120 nm and 260-480 HV respectively. Friction tests carried out using pin-on-plate method under normal loads of 10 N under ambient conditions showed values of the friction coefficient 0.25-0.40.

Keywords: chemical vapor deposition method, solid lubricant coating, molybdenum disulfide

1. Introduction

MoS_2 is a layered chalcogenide material that is an excellent solid lubricant and is widely used in high-precision space-borne applications such as satellite bearings, gears, and gimbals operating under extreme temperature ranges [1].

Super lubricity of MoS_2 is predetermined by its unique laminar structure characterized by low shear stress (≈ 25 MPa), which ensures extremely low friction coefficients (≈ 0.01). In MoS_2 , each Mo (IV) center is trigonal prismatic, being bound to six sulfide ligands, each of which is pyramidal. The trigonal prisms are interconnected to give a layered structure, wherein molybdenum atoms are sandwiched between layers of sulfur atoms. Because of the weak van der Waals interactions between the sheets of sulfide atoms, MoS_2 has a low coefficient of friction, resulting in excellent lubricating property [2,3]. Up to now, a large number of methods have been developed to prepare MoS_2 films, such as, Thermal diffusion [4], hydrothermal synthesis [5,6], physical vapor deposition [7], vertically aligned layers [8], photoluminescence [9], chemical vapor deposition (CVD) [10] and chemical deposition [11]. Recently, chemical vapor deposition (CVD) has been one of the most promising methods of producing high quality MoS_2 . Several precursors, such as $\text{Mo}(\text{St-Bu})_4$ and $\text{Ti}(\text{St-Bu})_4$ [12], MoO_3 [13], MoCl_5 [14], $\text{Mo}(\text{CO})_6$ [15], $(\text{NH}_4)_2\text{MoO}_2\text{S}_2$ and $(\text{NH}_4)_2\text{MoS}_4$ [16] have been used.

The sulfurization of MoO_3 using the CVD method has been adopted to synthesize MoS_2 . To our best knowledge, synthesis of

MoS_2 film onto steel substrates using a CVD method has not yet been reported. In this work, MoS_2 coatings using the MoO_3 and S precursors were deposited onto AISI 316 austenitic stainless steel and their properties were investigated.

2. Experimental

Samples of AISI 316 stainless steel, measuring 10 mm \times 5 mm \times 2 mm, were used as substrates. The composition of AISI 430 stainless steel is listed in Table 1. Specimens were polished with 320- up to 1200-grit paper, ultrasonically cleaned in ethanol and then dried.

TABLE 1
Chemical composition of AISI 316 stainless steel

Element	Fe	C	Cr	Mn	Si	S	P
Concentration (wt.%)	Bal	0.12	17.4	0.92	0.85	0.02	0.03

The CVD reactor (3Z.MTDI.900°C Modern Technology Development Institute) was used for deposition of the MoS_2 . Fig. 1 shows schematic illustrations of the reactor. As shown in Fig. 1 (a), 25 mg of MoO_3 powder (99%, Aldrich) and 600 mg of sulfur powder (99.5%, Alfa) were placed in two separate graphite crucibles and loaded separately into two furnaces, 1 and 2, to provide independent temperature control. To keep the substrate

* SHAHID BAHONAR UNIVERSITY OF KERMAN, FACULTY OF ENGINEERING, DEPARTMENT OF METALLURGY AND MATERIALS SCIENCE, JOMHOORI ESLAMI BLVD., KERMAN, IRAN

** SANAAT RESEARCH INSTITUTE, TEHRAN, IRAN

Corresponding author: m.zandrahimi@mail.uk.ac.ir

vertical, it was inserted into a holder and was placed in furnace 3. In order to remove air and steam in the reactor, argon gas with high purity (>99.99 %) was passed through the tube.

To avoid gradual sulfurization of MoO_3 powder by sublimated sulfur, a closed crucible was used for evaporation of MoO_3 powder. The heated MoO_3 powders were sublimed and swept by the Argon gas into the tube (see Fig. 1). Finally, the temperature of zones 1, 2 reached 200°C and 850°C respectively and were maintained for 180 min. However, temperature of zone 3 was 400, 500, 600 and 700°C . A fast cooling process with a 2 liter/min Ar was applied to stop the reaction quickly and control the growth time accurately.

Microstructure and chemical composition of the surface and cross section of coatings were analyzed using scanning electron microscopy (SEM) (Camscan MV2300) with energy dispersive spectroscopy (EDS). IR spectra were recorded in the $400\text{--}4000\text{ cm}^{-1}$ range with a resolution of 4 cm^{-1} , using Bruker tensor 27 FTIR spectrometer with RT-DLATGS detector and KBr pellet technique. X-ray diffraction (XRD) was used to identify the phases that formed in the surface layer of the coated sample, using $\text{Cu K}\alpha$ radiation ($\lambda = 1.5405\text{ \AA}$). Phase identification and Rietveld quantitative phase analysis were carried out using X'Pert High Score Plus v2.2 software.

The crystallite size was evaluated from X-ray diffraction patterns based on the Scherrer formula that is defined as:

$$\beta \cos \theta = K \lambda / d \quad (1)$$

Where β is the line broadening at half the maximum intensity (FWHM) in radians, λ is the wavelength, θ is the diffraction angle, and d is crystallite size [17].

The surface roughness was measured using stylus type (Talysurf Taylor Hobson) instruments. The average surface

roughness was measured at five different locations and results were averaged.

Friction tests were performed using a pin-on-disk machine. This equipment is controlled by its PC software, which allows observing the evolution of the friction coefficient. During the test, the treated samples were rotating against a stationary AISI 52100 steel pin (with 4.576 mm hemispherical tip radius and hardness of 800 HV30) at a linear speed of 0.11 m/s under loads of 10 N.

3. Results and discussion

Fig. 2 shows SEM images and EDX spectrums of coated samples prepared at deposition temperatures of 400°C and 700°C . As can be seen, coating fabricated at 400°C has flake structure and a rough surface ($R_a \approx 1.2\text{ }\mu\text{m}$) with many pores. This might be due to insufficient diffusion in deposition layers at this temperature. But as shown in Fig. 2b, the coating fabricated at 700°C hasn't flack structure, and is difficult to find pore on the surface of coating. Its surface roughness is $0.8\text{ }\mu\text{m}$. The resulting roughness of coatings at different substrate temperature is presented in Fig. 3. The coating roughness decreases with increasing substrate temperature. Change of surface roughness can be attributed to change in coating surface morphology caused by changes in substrate temperature.

Fig. 4 shows a cross section SEM image and EDS line scan of a coated specimen at 700°C . The thickness of coatings is about $30\text{ }\mu\text{m}$ no voids, pores or discontinuities is observed in the coating thickness. The Coating thickness as a function of substrate temperature is presented in Fig. 5. As can be seen the coating thickness increases with increasing substrate temperature, although the amount of thickness variation with temperature

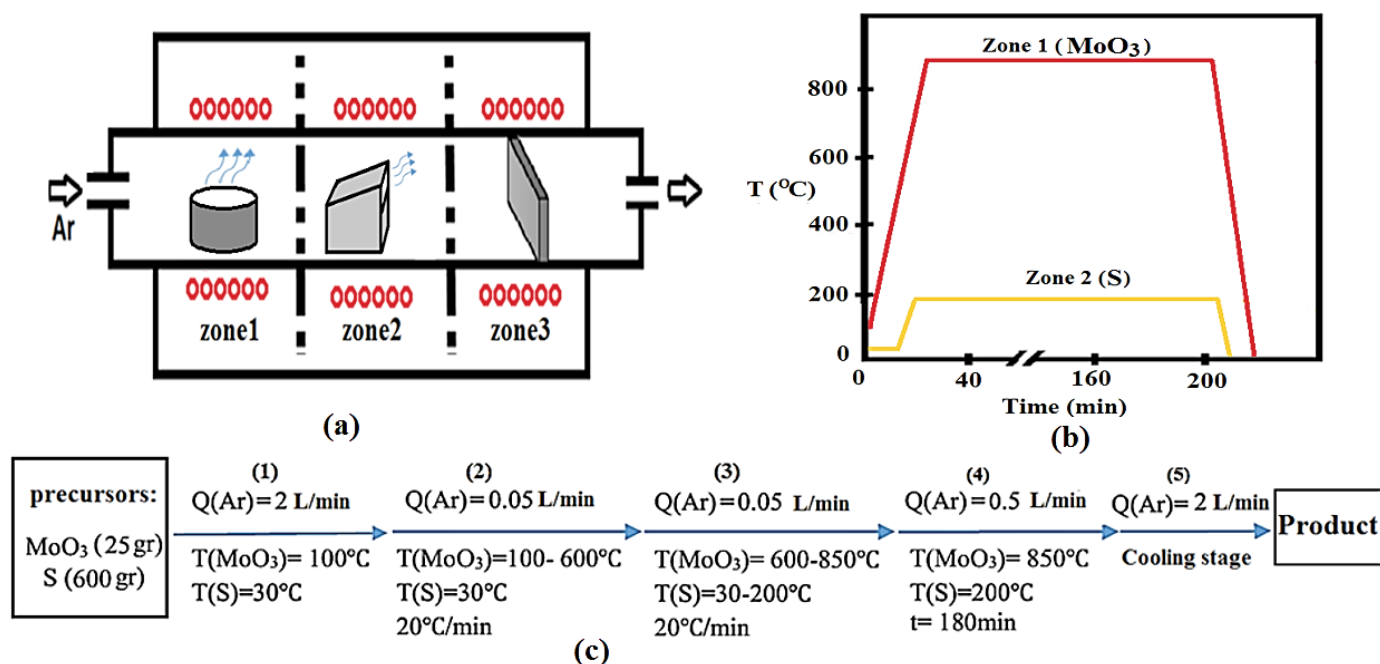


Fig. 1. (a) Schematic illustration of the MoS_2 CVD system. (b) Temperature programming process of MoO_3 and S precursors. (c) Flowchart showing the main steps of the MoS_2 programming process of MoO_3 and S precursors

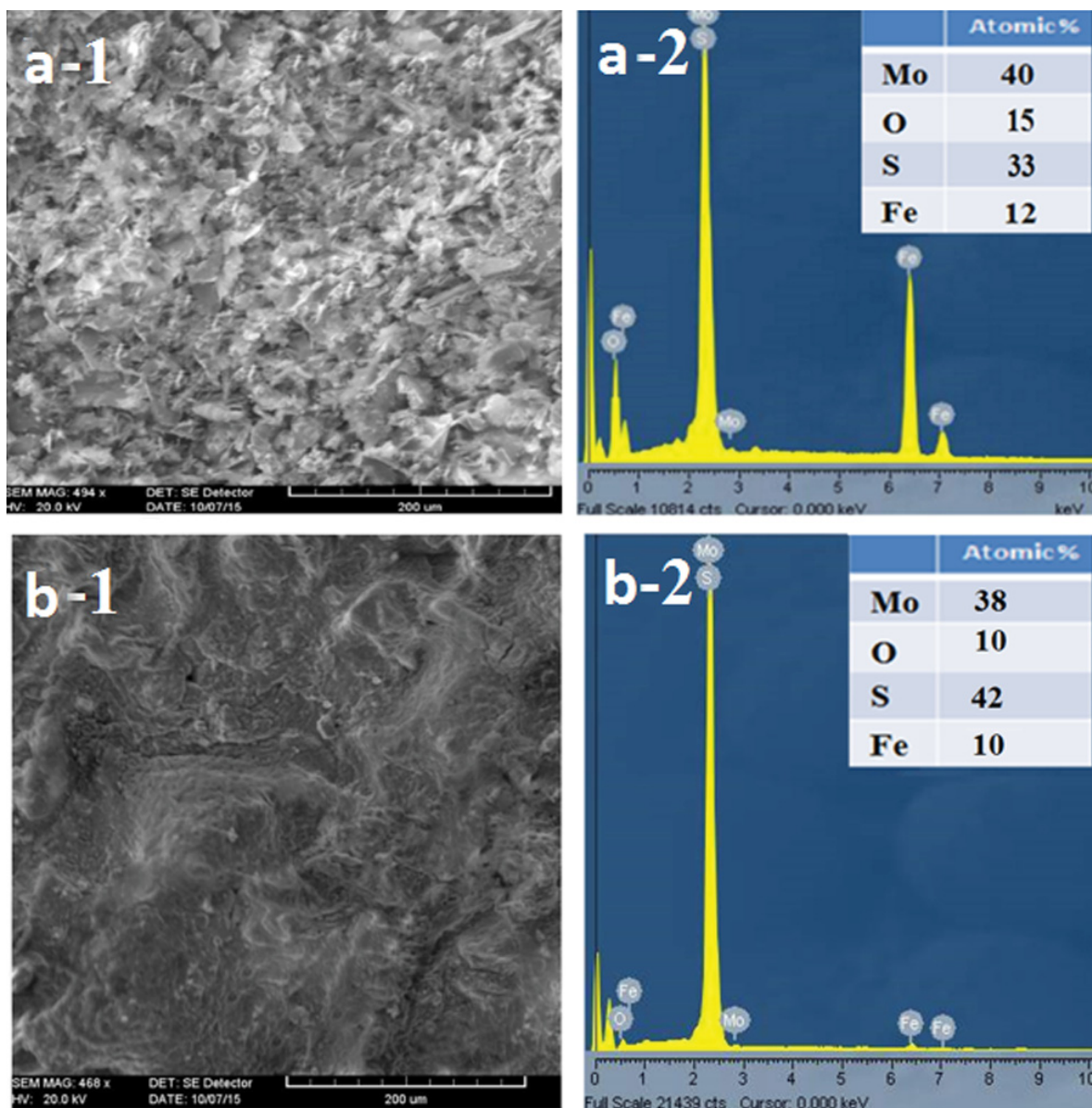


Fig. 2. SEM images and EDX spectrums of coated samples prepared at different temperatures deposition by CVD at: (a) 400°C and (b) 700°C, Inset shows the atomic percentage of the coatings

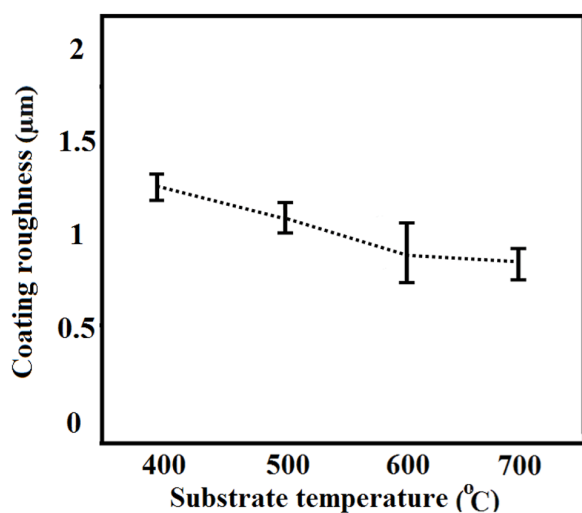


Fig. 3. The resulting roughness of coatings at different substrate temperatures

is small. During CVD the coating growth rate is limited by either surface reaction kinetics, mass transport (diffusion) of precursors to the substrate, or the feed rate of the precursors. By increasing the substrate temperature during the film deposition, as Fig. 6 depict, the mass transport and the surface reaction are influenced by the temperature. The surface reaction is the limiting step at lower temperature and mass transport is the rate limiting step at higher temperature. So the deposition temperatures used in this study is in the range of reaction temperature so that surface reaction is the limiting step [18,19].

The results of EDX analysis of surface of coated specimen with MoS₂ at different temperatures, are given in Table 2. As can be seen, the ratio of sulfur to oxide in the coating increases with increasing substrate temperature. Due to the endothermic reaction of MoO₃ with S, the amount of MoS₂ increases with increasing substrate temperature, the ratio of sulfur to oxide in the coating increases.

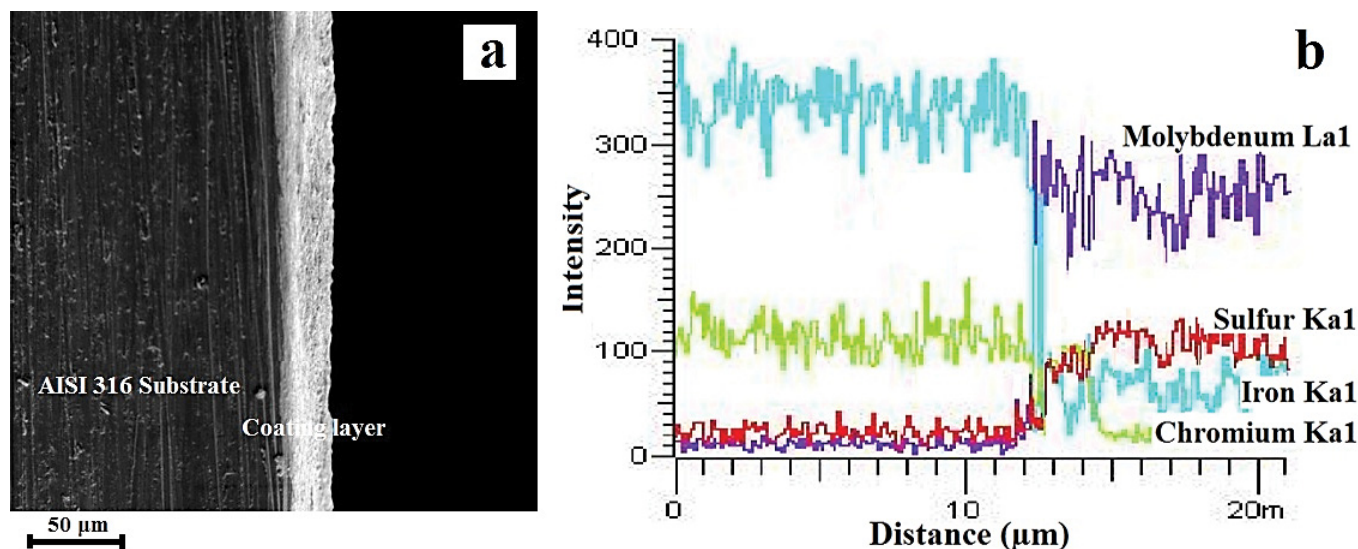


Fig. 4. SEM cross section image of coating fabricated at substrate temperature of 700°C (a) and EDS line scan (b)

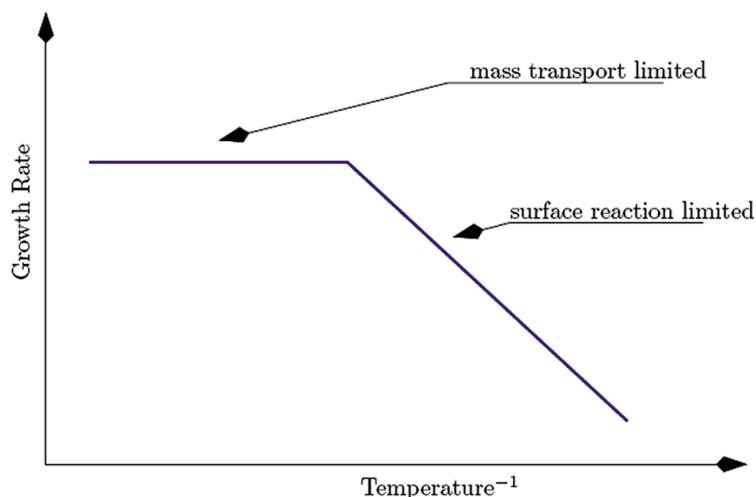


Fig. 5. The coating thickness as a function of substrate temperatures

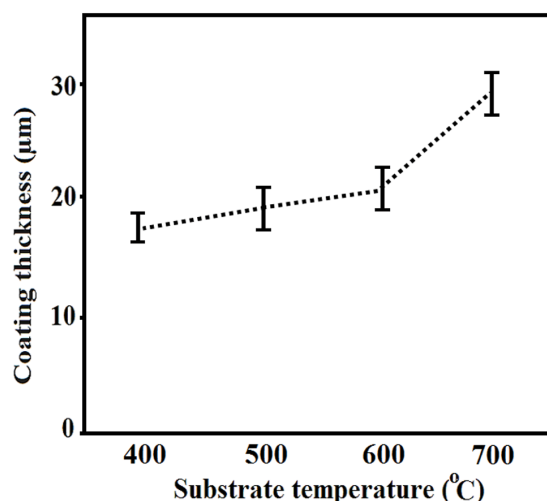


Fig. 6. Deposition rate as a function of temperature [17]

TABLE 2
Chemical composition of coating deposited by CVD process method at various substrate temperatures

Substrate temperature	Iron	Molybdenum	Sulfur	Oxygen	Sulfur/Oxygen ratio
400°C	12	40	33	15	2.2
500°C	11	38	39	12	3.25
600°C	12	41	37	10	3.7
700°C	10	38	42	10	4.2

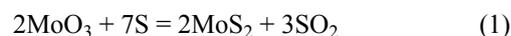
Cu K α radiation was employed to identify the phases formed in the surface layer of the specimens. Fig. 7 shows XRD diffraction patterns of CVD coatings at different substrate temperature. The identified phases include MoO₃, MoO₂ and MoS₂. These types of diffractometers have a high penetration depth, therefore the strong peaks originate from the substrate.

The strong diffraction peaks indicate that the product has good crystallinity. The results clearly show that the MoS₂ phase

is generated even at substrate temperature of 400°C. Diffraction peaks of MoS₂ phase can be indexed as the standard hexagonal MoS₂ phase by comparison with the data from JCPDS card no. 03-065-3656. The strong diffraction peaks at substrate temperatures of 400-700°C indicate that the products have good crystallinity.

As can be seen in Fig. 7 with increasing substrate temperature, diffraction peaks are strengthened slightly, indicating the improvement in crystallinity.

Fig. 8 shows the phase compositions obtained by Rietveld refinement of coatings at different substrate temperature. The reaction between MoO₃ and S is given in Eq. 1.



As can be seen in Fig. 8, there is significant amounts of MoO₂ in the coatings. Recent research indicates that the reaction of MoO₃ and S might also involve the stepwise reduction and sulfuration. Possible stepwise equations of the reaction can be described as follows:

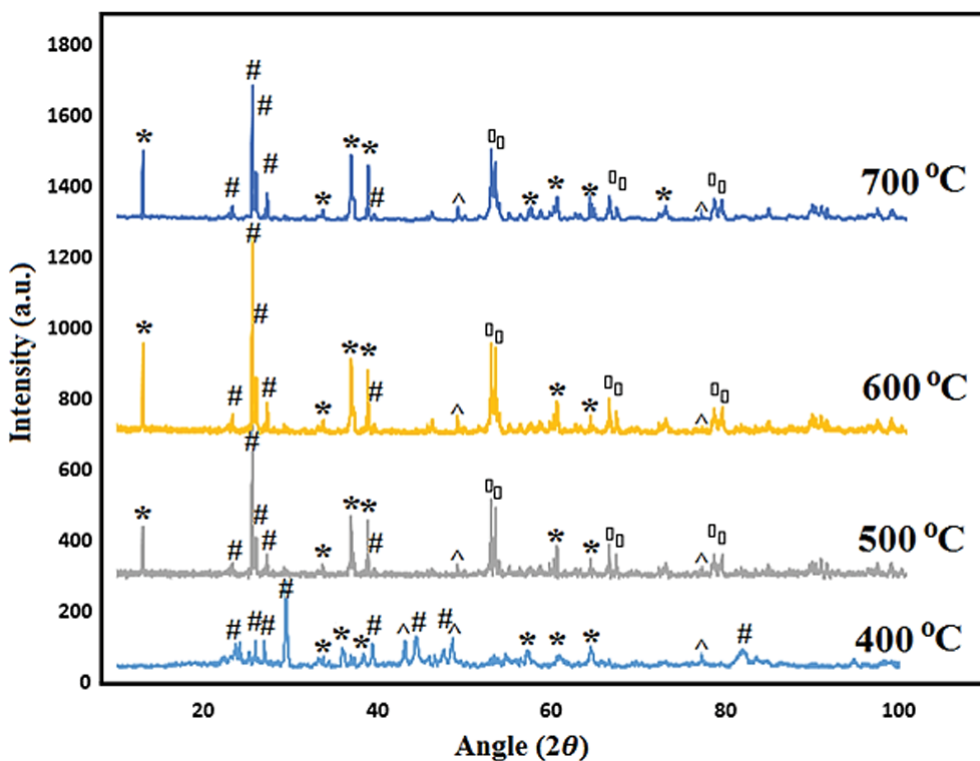
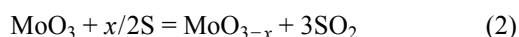


Fig. 7. XRD patterns of coating deposited by CVD process method at various substrate temperatures. (Symbol representations of the peaks: [*] MoS₂, [0] MoO₂, [^] MoO_{3-x} and [#] MoO₃)



MoO₂ is intermediate product and is one of the most stable in Mo compounds.

With the increase of substrate temperature from 400°C to 700°C, the presence of MoO₂ is significantly reduced and

MoS₂ is obtained dominantly. From these experiments, it can be concluded that the reaction occurs in two phases; in phase one, sulfur vapor reduces MoO₃ to MoO_{3-x}. In the second phase, the excess sulfur reacts with MoO_{3-x} and produces MoS₂. The temperature of process and reaction duration determines the degree of conversion of the MoO₃ into MoS₂ film [10,20,21].

The IR technique was used to verify the XRD assignments of oxide, sulfide species. The FT-IR spectrum of the coating is shown in Fig. 9. The relatively sharp bands at 974 and 911 cm⁻¹ are ascribed to the Mo = O characteristic stretching vibration of the hexagonal phase. The splitting peaks in 616 and 523 cm⁻¹ corresponds to the Mo-O vibration and the bands at 463 and 380 cm⁻¹ are ascribed to the Mo = S and Mo-S characteristic stretching vibration of the hexagonal phase which is in agreement which matched well with reference [22-24].

The grain size of the coatings is estimated based on the Scherrer formula from the X-ray diffraction patterns of (220) reflexes and are presented in Fig. 10. The grain size in coatings is subjected to various external conditions, among which the initial nucleation and growth of coating on the substrate may play a decisive role.

When the substrate temperature is increased from 400°C to 800°C, the surface mobility of the deposited atoms is further increased, so higher temperature promotes the grain size.

The resulting micro-Vickers hardness of coatings at different substrate temperature is presented in Fig. 11. As shown, the hardness increases with increasing substrate temperature up to a maximum of 450 HV at 500°C, then decreases progressively with increasing substrate temperature. In this process both phases

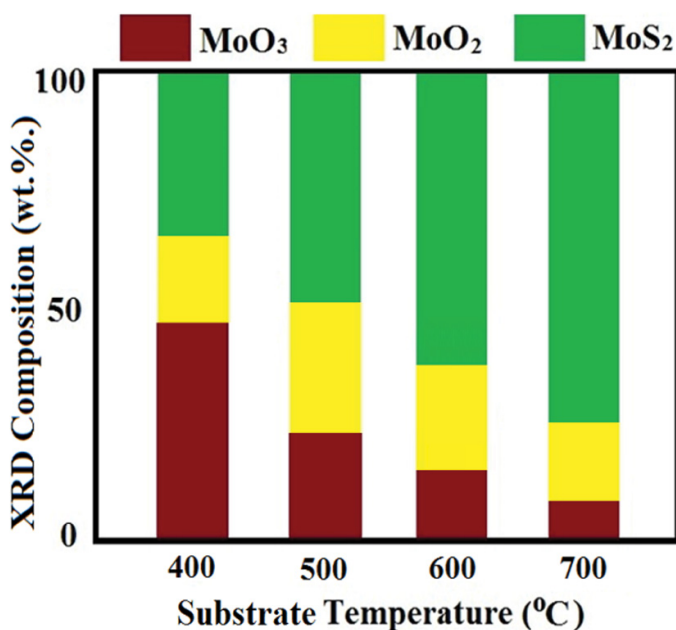


Fig. 8. Quantitative phase analysis data (wt.%) by the Rietveld Method for coatings at different substrate temperatures

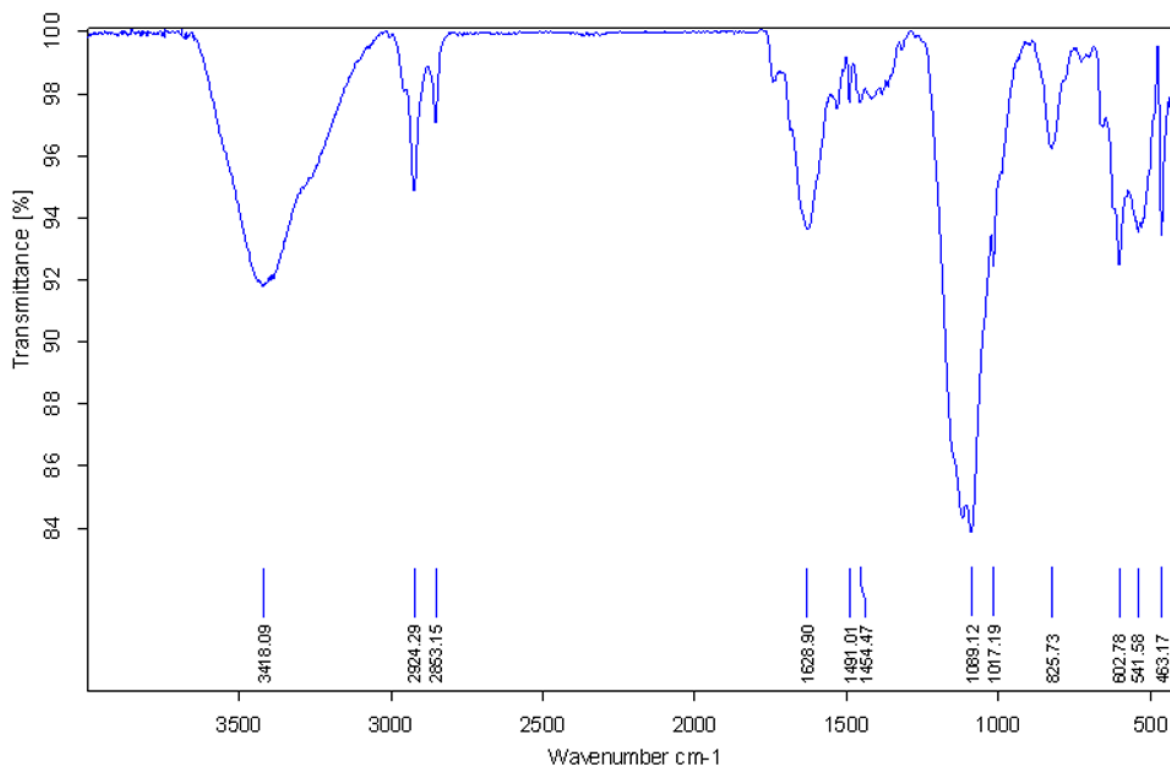


Fig. 9. FT-IR spectrum of coatings (at substrate temperature of 700°C)

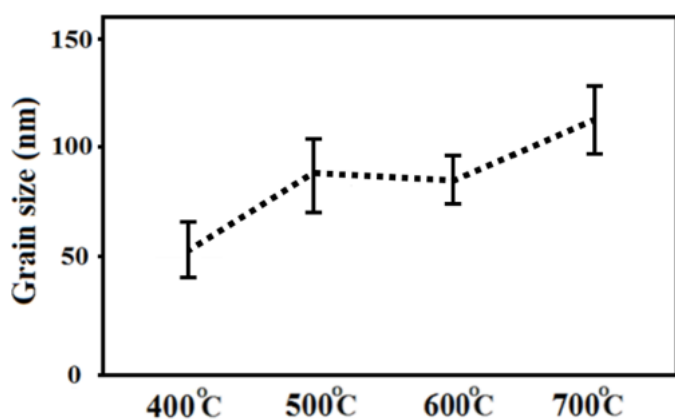


Fig. 10. The average grain size as a function of substrate temperature

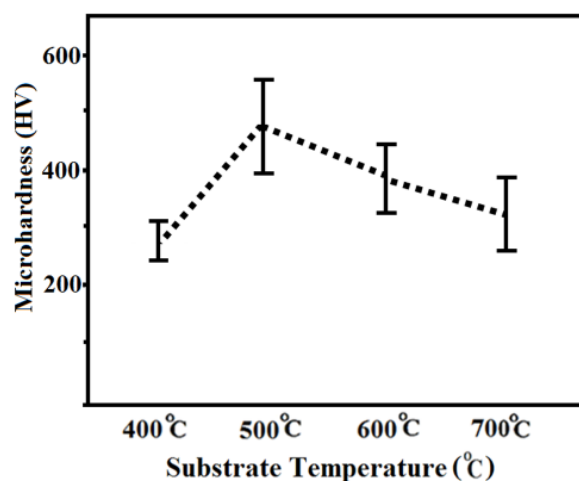


Fig. 11. The micro-Vickers hardness values of coatings at different substrate temperatures

produced and grain size of coatings are the two main factors that affect the hardness. The dependence of material hardness on the grain size can be described by the phenomenological “Hall-Petch” equation [25], as follows:

$$H_v = H_0 + Kd^{-0.5} \quad (4)$$

Where, H_v is the measured hardness, H_0 is the intrinsic hardness dependent on frictional lattice resistance to dislocation motion, k is the material-specific strengthening coefficient, and D is the average grain size. This relationship is based on the observation that grain boundaries impede dislocation movement and that the number of dislocations within a grain have an effect on how easily dislocations can traverse grain boundaries and travel from

grain to grain. According to Hall-Petch relationship, the decrease in grain size leads to hardness enhancement. But as can be seen from Fig. 11, the hardness of coating increases with increasing coating grain size from substrate temperature of 400°C to 500°C. According to the phase composition, MoO_2 phase is at maximum value at different deposition temperatures (Fig. 7). Since MoO_2 is harder than MoS_2 and MoO_3 (The Mohs-scale hardness values of MoS_2 , MoO_3 and MoO_2 are 1.59, 2.55 and 4.64, respectively [26-28]), the hardness is increased at 500°C but because of increasing grain size and decreasing MoO_2 phase in coating, the hardness is decreased with increasing of substrate temperature in the range of 500-700°C.

The variation of the steady state friction coefficient of the coatings and substrate is presented in Fig. 12. It is observed that the values of the friction coefficient increases with the decrease of substrate temperatures and is in the range of 0.25-0.40. As can be seen in Fig. 8 with the increase of substrate temperature the presence of MoS₂ as an ultra-lubricant phase is significantly increased, so coating friction coefficient decreases with increasing substrate temperature.

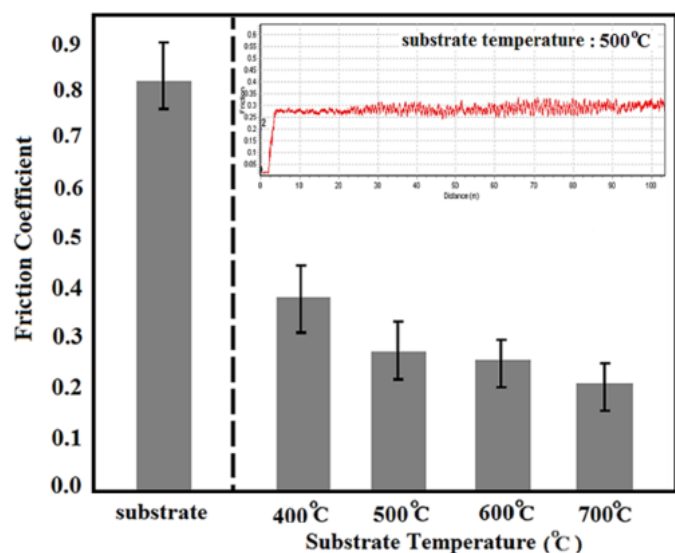


Fig. 12. The friction coefficient values of coatings at different substrate temperatures. Inset shows the friction coefficient of the coating at substrate temperatures of 500°C.

4. Conclusions

MoS₂ coating was successfully fabricated on the AISI 316 austenitic stainless steel, using vapor deposition. A mixture of MoS₂ and molybdenum dioxide (MoO₂) was produced by evaporating sulfur powder and molybdenum trioxide (MoO₃). In this method, temperatures less than 850°C was used which is much lower than the temperature, required for the direct evaporation of MoS₂. A mixture of MoS₂ and molybdenum dioxide (MoO₂) was produced. The results displayed the progress of MoS₂ formation from MoO₂ which is in correspondence with temperature. The coating layer had compact and dense morphology. The thickness, grain size and the hardness of the coating were 17-29 μm, 50-120 nm and 260-480 HV respectively. Pin-on-plat reciprocating tests demonstrated the coating friction coefficient 0.25-0.40 (20°C, air).

Acknowledgment

This research has been done by the cooperation of the Sanaat Research Institute and the authors wish to thank this Institute for providing the research funding.

REFERENCES

- [1] J. Yang, Y. Jiang, J. Hardell, B. Prakash, Influence of service temperature on tribological characteristics of self-lubricant coatings: A review, *Front. Mater. Sci.* **7**, 28-39 (2013).
- [2] A.R. Lansdown, *Molybdenum Disulphide Lubrication*, 1999 Elsevier.
- [3] Wang, Haidou, Binshi Xu, Jiajun Liu, *Micro and nano sulfide solid lubrication*, 2013 Springer Science and Business Media.
- [4] O. Smorygo, S. Voronin, P. Bertrand, I. Smurov, Fabrication of thick molybdenum disulphide coatings by thermal-diffusion synthesis, *Tribol. Lett.* **17**, 723-726 (2004).
- [5] Y. Peng, Z. Meng, C. Zhong, J. Lu, W. Yu, Y. Jia, Y. Qian, Hydrothermal Synthesis and Characterization of Single-Molecular-Layer MoS₂ and MoSe₂, *Chem. Lett.* **9**, 772-773 (2001).
- [6] H. Luo, C. Xu, D. Zou, L. Wang, T. Ying, Hydrothermal synthesis of hollow MoS₂ microspheres in ionic liquids/water binary emulsions, *Mater. Lett.* **62**, 3558-3560 (2008).
- [7] C. Gong, C. Huang, J. Miller, L. Cheng, Y. Hao, D. Cobden, J. Kim, R.S. Ruoff, R.M. Wallace, K. Cho, Metal contacts on physical vapor deposited monolayer MoS₂, *ACS nano.* **7**, 11350-11357 (2013).
- [8] D. Kong, H. Wang, J.J. Cha, M. Pasta, K.J. Koski, J. Yao, Y. Cui, Synthesis of MoS₂ and MoSe₂ films with vertically aligned layers, *Nano letters* **13**, 1341-1347 (2013).
- [9] Q. Ji, Y. Zhang, T. Gao, Y. Zhang, D. Ma, M. Liu, Y. Chen, X. Qiao, P.-H. Tan, M. Kan, Epitaxial monolayer MoS₂ on mica with novel photoluminescence, *Nano lett.* **13**, 3870-3877 (2013).
- [10] Y.H. Lee, X.Q. Zhang, W. Zhang, M.T. Chang, C.T. Lin, K.D. Chang, Y.C. Yu, J.T.W. Wang, C.S. Chang, L.J. Li, Synthesis of Large-Area MoS₂ Atomic Layers with Chemical Vapor Deposition, *Adv. Mater.* **24**, 2320-2325 (2012).
- [11] P. Pramanik, S. Bhattacharya, Deposition of molybdenum chalcogenide thin films by the chemical deposition technique and the effect of bath parameters on these thin films, *Mater. Res. Bull.* **25**, 15-23 (1990).
- [12] J. Cheon, J.E. Gozum, G.S. Girolami, Chemical Vapor Deposition of MoS₂ and TiS₂ Films From the Metal-Organic Precursors Mo(S-t-Bu)₄ and Ti(S-t-Bu)₄, *Chem. Mater.* **9**, 1847-1853 (1997).
- [13] G. Cai, J. Jian, X. Chen, M. Lei, W. Wang, Regular hexagonal MoS₂ microflakes grown from MoO₃ precursor, *Appl. Phys. A* **89**, 783-788 (2007).
- [14] R. Browning, P. Padigi, R. Solanki, D.J. Tweet, P. Schuele, D. Evans, Atomic layer deposition of MoS₂ thin films, *Mater. Res. Express* **2**, 35006 (2015).
- [15] M.R. Close, J.L. Petersen, E.L. Kugler, Synthesis and characterization of nanoscale molybdenum sulfide catalysts by controlled gas phase decomposition of Mo(CO)₆ and H₂S, *Inorg. Chem.* **38**, 1535-1542 (1999).
- [16] K. He, S. Zhang, J. Mi, J. Chen, L. Cheng, Mechanism of catalytic hydrolysis of sedimentary organic matter with MoS₂, *Pet. Sci.* **8**, 134-142 (2011).
- [17] U. Holzwarth, N. Gibson, The Scherrer equation versus the 'Debye-Scherrer equation', *Nat. Nanotechnol.* **6**, 534-534 (2011).

- [18] J.H. Park, T.S. Sudarshan, *Chemical Vapor Deposition*, 2001 ASM International.
- [19] A. Pierson, O. Hugh, *Handbook of Chemical Vapor Deposition (CVD) (Second Edition)*, William Andrew Publishing, 1999 Norwich.
- [20] H. Schmidt, S. Wang, L. Chu, M. Toh, R. Kumar, W. Zhao, A.H. Castro Neto, J. Martin, S. Adam, B. Ozyilmaz, Transport properties of monolayer MoS₂ grown by chemical vapor deposition, *Nano Lett.* **14**, 1909-1913 (2014).
- [21] X. Wang, H. Feng, Y. Wu, L. Jiao, Controlled synthesis of highly crystalline MoS₂ flakes by chemical vapor deposition, *J. Am. Chem. Soc.* **135**, 5304-5307 (2013).
- [22] I.G. Vasilyeva, I.P. Asanov, L.M. Kulikov, Experiments and Consideration about Surface Nonstoichiometry of Few-Layer MoS₂ Prepared by Chemical Vapor Deposition, *J. Phys. Chem.* **119**, 23259-23267 (2015).
- [23] F. Maugé, J. Lamotte, N. Nesterenko, O. Manoilova, A. Tsyganenko, FT-IR study of surface properties of unsupported MoS₂, *Catal. today* **70**, 271-284 (2001).
- [24] L.Q. Mai, B. Hu, W. Chen, Y. Qi, C. Lao, R. Yang, Y. Dai, Z.L. Wang, Lithiated MoO₃ nanobelts with greatly improved performance for lithium batteries, *Adv. Mater.* **19**, 3712-3716 (2007).
- [25] A. Chokshi, A. Rosen, J. Karch, H. Gleiter, On the validity of the Hall-Petch relationship in nanocrystalline materials, *Scr. Metall.* **23**, 1679-1683 (1989).
- [26] H.P. Martinz, B. Nigg, Surface Hardened Molybdenum Alloys for the Processing of Polymers, *Surface Modification Technologies: Proceedings of the 20th International Conference on Surface Modification Technologies*, ASM International, 2007.
- [27] J. Panitz, L. Pope, J. Lyons, D. Staley, The tribological properties of MoS₂ coatings in vacuum, low relative humidity, and high relative humidity environments, *J. Vac. Sci. Technol. A* **6**, 1166-1170 (1988).
- [28] Y. Takeichi, T. Chujo, N. Okamoto, M. Uemura, Effects of Molybdenum Trioxide on the Tribological Properties of Aluminum Bronze under High Temperature Conditions, *Tribology Online* **4**, 135-139 (2009).